Atmos. Chem. Phys., 8, 7239–7254, 2008
www.atmos-chem-phys.net/8/7239/2008/

Atmospheric Chemistry and Physics

Mechanisms for synoptic variations of atmospheric CO_2 in North America, South America and Europe

N. C. Parazoo[1], A. S. Denning[1], S. R. Kawa[2], K. D. Corbin[1], R. S. Lokupitiya[1], and I. T. Baker[1]

[1]Atmospheric Science Department, Colorado State University, Fort Collins, Colorado, USA
[2]NASA Goddard Space Flight Center, Greenbelt, Maryland, USA

Received: 15 April 2008 – Published in Atmos. Chem. Phys. Discuss.: 20 June 2008
Revised: 4 November 2008 – Accepted: 4 November 2008 – Published: 10 December 2008

Abstract. Synoptic variations of atmospheric CO_2 produced by interactions between weather and surface fluxes are investigated mechanistically and quantitatively in midlatitude and tropical regions using continuous in-situ CO_2 observations in North America, South America and Europe and forward chemical transport model simulations with the Parameterized Chemistry Transport Model. Frontal CO_2 climatologies show consistently strong, characteristic frontal CO_2 signals throughout the midlatitudes of North America and Europe. Transitions between synoptically identifiable CO_2 air masses or transient spikes along the frontal boundary typically characterize these signals. One case study of a summer cold front shows CO_2 gradients organizing with deformational flow along weather fronts, producing strong and spatially coherent variations. In order to differentiate physical and biological controls on synoptic variations in midlatitudes and a site in Amazonia, a boundary layer budget equation is constructed to break down boundary layer CO_2 tendencies into components driven by advection, moist convection, and surface fluxes. This analysis suggests that, in midlatitudes, advection is dominant throughout the year and responsible for 60–70% of day-to-day variations on average, with moist convection contributing less than 5%. At a site in Amazonia, vertical mixing, in particular coupling between convective transport and surface CO_2 flux, is most important, with advection responsible for 26% of variations, moist convection 32%, and surface flux 42%. Transport model sensitivity experiments agree with budget analysis. These results imply the existence of a recharge-discharge mechanism in Amazonia important for controlling synoptic variations of boundary layer CO_2, and that forward and inverse simulations should take care to represent moist convective transport. Due to the scarcity of tropical observations at the time of this study, results in Amazonia are not generalized for the tropics, and future work should extend analysis to additional tropical locations.

Correspondence to: N. C. Parazoo
(nparazoo@atmos.colostate.edu)

1 Introduction

An important method for estimating net sources and sinks of carbon is through tracer transport inversion, where atmospheric CO_2 concentrations (hereafter denoted CO_2) and a transport model are combined to infer surface CO_2 flux (hereafter denoted surface flux) patterns (Gurney et al., 2002; Rödenbeck et al., 2003; Baker et al., 2006). With more continuous in-situ CO_2 surface observations available around the world, inversions can integrate high frequency measurements to improve flux estimation. These continental measurements contain short-term diurnal and synoptic (day-to-day) variations strongly influenced by coupling between weather and surface flux (e.g., Law et al., 2002; Gerbig et al., 2003; Geels et al., 2004; Lin et al., 2004; Peylin et al., 2005; Lauvaux et al., 2008). Global and regional models of the atmosphere must capture the heterogeneous nature of transport and surface flux (Geels et al., 2004; Wang et al., 2007) in order to quantify regional scale CO_2 sources and sinks with any certainty.

Coupling between weather and surface flux helps create day-to-day variations in boundary layer CO_2 such as those of Fig. 1, which shows mid-afternoon planetary boundary layer (PBL) CO_2 – given as a mole fraction in units of parts per million (ppm) – from sites in North America, South

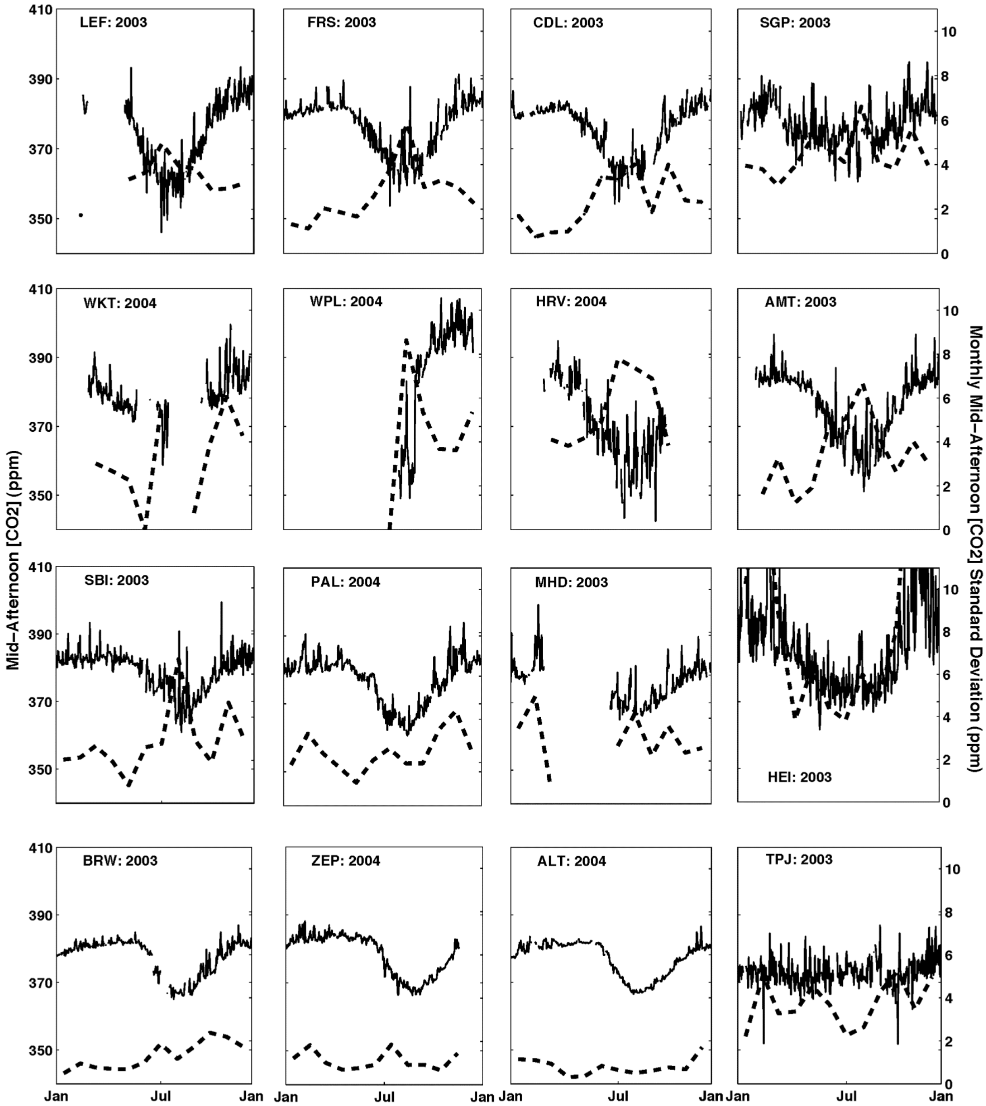

Fig. 1. Mid-afternoon CO_2 (ppm) at in-situ continuous sites (solid, left y-axis) and monthly standard deviation of mid-afternoon values (dashed, right-y-axis) for 1 year. Station and corresponding year are labeled within plot. The locations of these stations are shown in Fig. 2.

America and Europe. Mid-afternoon is chosen because the amount of regional and synoptic influence on tracer concentrations within well-mixed boundary layers is maximized during this time (Bakwin et al., 1998). Synoptic variations of 10–20 ppm over 1–3 days are common, comparable to seasonal amplitudes. Continental variations under terrestrial influence are frequently much stronger than variations in remote mountainous and maritime locations (e.g., Patra et al., 2008). Comparison of monthly standard deviation of mid-afternoon values at continental (e.g., LEF, HRV, and HEI) and remote (e.g., ALT, BRW, and ZEP) sites confirms this (Fig. 1). These variations are large and must be reproduced properly, in timing and magnitude, in model simulations.

Davis et al. (2003) observe that daily PBL CO_2 tendencies at a site in the northern part of the United States are governed primarily by local net ecosystem exchange (NEE, defined as gross primary production minus ground respiration) during fair weather. During the seasonal transition months of May and September, however, the sign of NEE is contradictory to CO_2 tendencies expected from NEE of CO_2. Preliminary investigation explained this through the presence of discrete non-fair weather events such as frontal passage.

Mechanisms proposed in the literature to explain synoptic variations during frontal passage include (see Geels et al., 2004): (1) nonlocal influence through lateral advection of upstream horizontal CO_2 gradients (e.g., Worthy et al., 2003; Chan et al., 2004; Geels et al., 2004; Corbin and Denning, 2006); (2) vertical mixing through moist convection and frontal lifting over air mass boundaries along frontal zones (e.g., Chan et al., 2004); and (3) ecosystem respiration and photosynthesis response to frontal weather (e.g., Chan et al., 2004). These studies show that horizontal advection of remotely generated CO_2 anomalies is an important source for downstream variations. Additionally, Chan et al. (2004) show that biospheric fluxes are strongly coupled to radiative forcing changes under cloud cover associated with fronts.

Although most of the sites shown in Fig. 1 are in midlatitudes, it is interesting that the magnitude of day-to-day variations at the one tropical site, TPJ, is on the same order as those in midlatitudes. It is well known that the nature of weather in Amazonia is much different from that of midlatitudes. This is explained in part by the different energetics of the atmosphere. In the tropical atmosphere of Amazonia, latent heat release associated with cumulus convection is the significant source of energy for weather (Holton, 1992). Although latent heat is important in midlatitudes, it is generally thought to be a secondary energy source for synoptic weather. Midlatitude synoptic scale weather disturbances derive energy from the zonal available potential energy associated with latitudinal temperature gradients (baroclinicity). In Amazonia, because of weak temperature gradients and negligible Coriolis effect, baroclinic effects are weak. Due to thermodynamic constraints, horizontal mixing is more prevalent in midlatitudes while vertical convective mixing is more prevalent in Amazonia. These differences in weather play an important role in controlling synoptic CO_2 variations.

Studies have shown the need for accurate forward modeling of atmospheric transport as a requisite for reliable inverse estimate of surface flux (e.g., Gurney et al., 2003). This study investigates and quantifies physical (transport by advection and moist convective mixing) and biological (surface sources and sinks due to vegetative uptake/emission and anthropogenic emission) mechanisms responsible for synoptic variations of CO_2 in midlatitudes and Amazonia using well-calibrated continuous observations from 17 sites across the globe, global transport model simulations, and boundary layer budget analysis. The remainder of the paper is organized as follows: Sect. 2 describes the simulation models and CO_2 observations, Sect. 3 discusses the observed and simulated synoptic variations at sites in North America, South America, and Europe, and Sect. 4 summarizes key findings.

2 Methods

2.1 Observations

Continuous CO_2 observations are utilized to investigate day-to-day temporal variations at a point in space. These data are collected at hourly resolution from well-calibrated continuous stations in North America, South America, and Europe. Although the range of measurement heights varies from 9–457 m above the ground, only measurements between 9–40 m are included in the analysis for consistency. Figure 2 shows the location of each site. Table 1 gives a brief description and references for each site. Descriptions of the majority of these sites, in addition to some data access, can also be found at http://www.esrl.noaa.gov/gmd/ccgg/index.html and http://gaw.kishou.go.jp/wdcgg/.

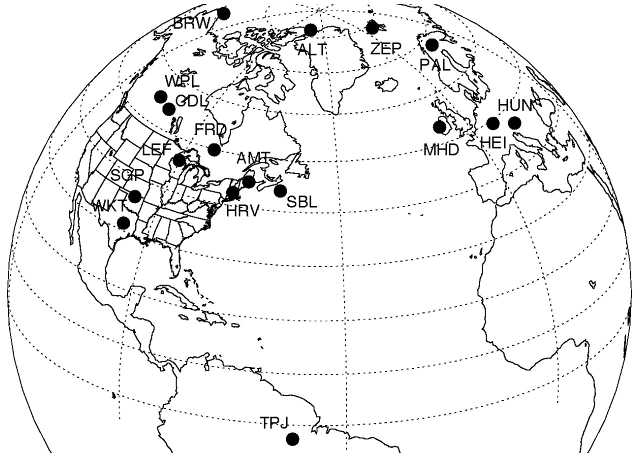

Fig. 2. Map of in-situ continuous sites.

Many of the observations contain large diurnal cycles, especially during the summer and in Amazonia. The diurnal cycle is a result of covariance between atmospheric mixing processes and surface exchange with the biosphere (the so-called rectifier effect). Law et al. (2008) analyze simulated diurnal cycles across a range of chemical transport models and find that amplitude errors can be attributed to site location (e.g., remote, island, mountain, coastal, and continental sites), altitude, model vertical resolution, sampling choice in the vertical and horizontal, choice of land surface flux, and subgrid-scale spatial heterogeneity in surface flux. These errors are amplified during stable nocturnal boundary layers, when surface emissions of CO_2 become strongly stratified in the vertical. This situation creates strong vertical gradients near the surface that are difficult for models to resolve. On the contrary, the daytime convective PBL creates a well-mixed boundary layer such that CO_2 mixing ratios near the surface are similar to those near the PBL top (Bakwin et al., 1998). Because stable nocturnal conditions make variations near the surface difficult to simulate, only mid-afternoon observations and model output are utilized in this study. CO_2 is averaged from 01:00–05:00 p.m. local time when the PBL is assumed to be near its maximum depth.

2.2 Models and driver data

The Parameterized Chemistry Transport Model (PCTM) is used for forward global simulations of CO_2 transport (e.g., Kawa et al., 2004). This provides a diagnostic tool for studying synoptic interactions among weather and surface flux. Transport fields are provided by NASA's Goddard Earth

Table 1. Description of Continuous Sites. Station ID corresponds with locations in Fig. 2.

Station ID	Station Name	Station Description
LEF	Park Falls	Northern Wisconsin; surrounded by mixed forest, wetlands, agriculture, and heavy population to the SE (Bakwin et al., 1998)
FRS	Fraserdale	South of the Hudson Bay Lowland and north of the boreal forest (Higuchi et al., 2003)
SGP	Southern Great Plains	Great Plains of North America in a region of strong moisture gradients, characterized by agriculture (Sims and Bradford, 2001)
WKT	Moody	Great Plains of North America in a region of strong moisture gradient, characterized by cattle grazing (NOAA GMD)
WPL	Western Peatland	Southern boreal forest of Canada (Syed et al., 2006)
CDL	Candle Lake	Southern boreal forest of Canada (WDCGG)
HRV	Harvard Forest	Northeastern United States; characterized by deciduous forest and heavy population to the south (Barford et al., 2001)
AMT	Argyle	Northeastern United States; characterized by deciduous forest and heavy population to the south (NOAA GMD)
TPJ	Tapajos	Tapajos National Forest in the Amazon Basin (Goulden et al., 2004)
ALT	Alert	Northeastern tip of Ellesmere Island in Nunavut, remote from major industrial regions (Worthy et al., 1998)
BRW	Barrow	Alaskan coast of the Arctic Ocean, remote from major industrial regions (WDCGG)
PAL	Pallas	Northern Finland in the subarctic at the northern limit of the northern boreal forest zone (Eneroth et al., 2005)
SBI	Sable Island	Island off the coast of Nova Scotia influenced by anthropogenic and terrestrial airflow of North America (Worthy et al., 2003)
MHD	Mace Head	West coast of Ireland with westerly exposure to the North Atlantic Ocean (Biraud et al., 2002)
ZEP	Zeppelin	Mountain ridge in the European Arctic off the western coast of Spitsbergen (Stohl et al., 2006)
HEI	Heidelberg	Germany, fairly strong industrial influence to the east (Gamnitzer et al., 2006)
HUN	Hungary	Western Hungary, flat region surrounded by agriculture and patchy forest (Haszpra et al., 2001)

Observation System, version 4 (GEOS4), data assimilation system (GEOS4-DAS) (Bloom et al., 2005) and include 6-hourly analyzed winds, temperatures, diffusion coefficients, and convective mass fluxes. GEOS4-DAS is built around the finite-volume general circulation model based on the Lin-Rood dynamical core (Lin and Rood, 1998). Physical parameterizations are derived from the National Center for Atmospheric Research Community Climate Model, Version 3 (Kiehl et al., 1998). Subgrid scale vertical processes include cumulus convection (cloud mass flux from deep (Zhang and McFarlane, 1995) and shallow (Hack, 1994) parameterized convection) and turbulence parameters. Non-conservation of mass in the data assimilation process, important for studies of tracer transport, is resolved through a “pressure fixer” procedure (see Kawa et al., 2004).

Surface sources and sinks include hourly NEE from the Simple Biosphere Model, Version 3 (SiB3), constant in time anthropogenic fossil fuel emissions (Andres et al., 1996), and monthly air-sea exchange of CO_2 (Takahashi et al., 2002). Fire emissions are ignored. SiB3 is a land-surface parameterization scheme originally used to simulate biophysical processes in climate models (Sellers et al., 1986), but later adapted to include ecosystem metabolism (Sellers et al., 1996; Denning et al., 1996). SiB3 involves the direct calculation of carbon assimilation by photosynthesis to calculate land-atmosphere CO_2 exchange (Denning et al., 1996; Sellers et al., 1996). The soil representation is similar to that of the Common Land Model (see Dai et al. 2003), with 10 soil layers and an initial soil column depth of 3.5 m. Temperature, moisture, and trace gases are calculated prognostically in the canopy air space. SiB3 has been evaluated against eddy covariance measurements at a number of sites (Baker et al., 2003; Hanan et al., 2005; Vidale and Stockli, 2005).

SiB3 is run in steady state mode in which ecosystem respiration balances gross primary production (Denning et al., 1996) over one year at every grid point. This eliminates long-term sources and sinks. The meridional gradient and secular trends simulated by the model are therefore stronger than observed (Kawa et al., 2004), but this study focuses on synoptic time scales. Flux and energy calculations in SiB3 are driven by GEOS4-DAS meteorology for the same time period as PCTM such that transport and surface flux are synchronized.

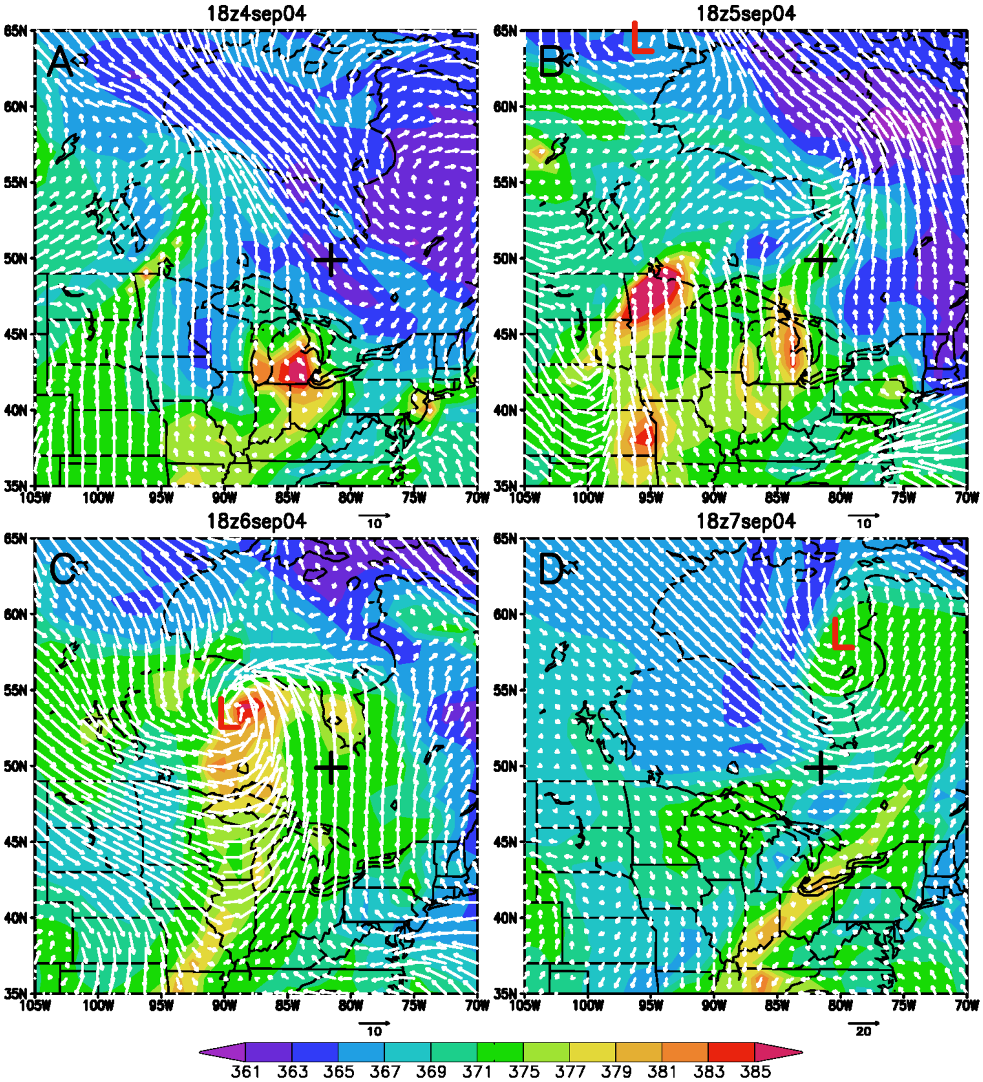

Fig. 3. Simulated evolution of daytime CO_2 surface anomalies (color contours given in ppm) with surface winds (white vectors) over 4-day period from 4–7 September 2004. All snapshots occur at 18 GMT. Day 1 corresponds to panel **(A)** (4 September), day 2 to **(B)** (5 September), day 3 to **(C)** (6 September), and day 4 to **(D)** (7 September). The red L represents a cyclonic low-pressure center. The black cross indicates the location of FRS.

GEOS4-DAS precipitation is scaled by monthly precipitation from the Global Precipitation Climatology Project (GPCP) (Huffman et al., 2001) to force total monthly precipitation in GEOS4-DAS to match that of GPCP. The time at which precipitation occurs remains unchanged so that covariance of anomalies in cloudiness, moisture, and vertical transport is conserved.

Details of PCTM and the experimental setup are similar to Kawa et al. (2004). PCTM is run from 2000–2004 at 1.25° by 1° (longitude by latitude) with 25 levels to 1 mbar, where 2000–2002 comprised the spin up period to establish the interhemispheric CO_2 gradient. CO_2 is treated as a passive tracer, with the time rate of decay ignored at synoptic scales and the small source from CO oxidation assumed to be included in the surface emissions. The CO_2 distribution is therefore determined only by transport from surface sources and removal by surface sinks.

3 Results and discussion

As discussed in Sect. 1, frontal passage events in the spring and autumn cause CO_2 variations that are inconsistent with local NEE. It is well known that any tracer tends to align along the deformation axis of temperature fronts. This is because sharp temperature gradients exist along fronts and it is natural for long-lived tracers such as CO_2 to experience similar contrasts. This is important for interpretation of high frequency CO_2 observations, which experience strong and

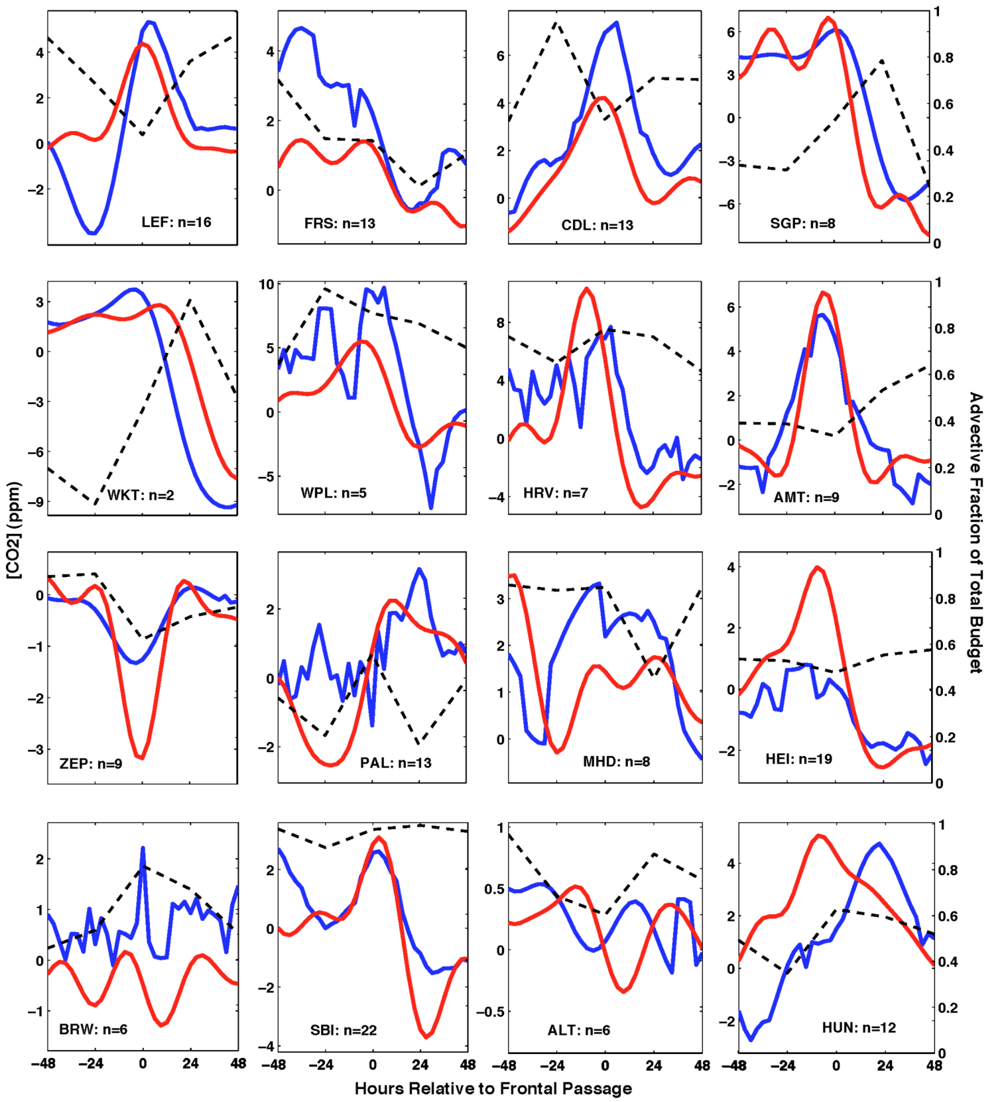

Fig. 4. (Left Y-Axis) Summer (June–July–August–September) climatology of observed (blue) and simulated (red) frontal CO_2. (Far Right Y-Axis) Total fractional contribution of advective tendencies computed from budget analysis (black dashed lines). Climatologies created using method described in Sect. 3.2. The time of frontal passage is denoted by 0 on the x-axis. The station and number of events used in the averaging (n) is indicated within each plot.

sudden variations (see Fig. 1) as a consequence of large-scale dynamics (rather than strictly local processes) in which instabilities in the general circulation lead to formation of surface fronts. These fronts work on CO_2 gradients near the surface and transport CO_2 anomalies across the continent. This type of information is important for carbon modelers who wish to utilize hourly CO_2 observations. Ignoring diurnal variations, these events are the dominant source of variance in midlatitude CO_2 observations, creating the synoptic "signal" seen in Fig. 1. It is therefore necessary to quantitatively explain them if inverse analysis is to be valid. The following discussion, followed by sensitivity experiments using PCTM, explores these variations quantitatively and qualitatively.

Examples of deformational flow along cold fronts and resulting frontal CO_2 variations are discussed in Sect. 3.1 and 3.2. These variations are then broken down through budget analysis in Sect. 3.3. Analysis is generalized to all transport events in midlatitudes and Amazonia in Sect. 3.4.

3.1 Deformational flow

As is shown in Sect. 3.2, transient variations are common during frontal passage. These variations are easily seen in snapshots of simulated CO_2. An example of this, near Fraserdale, is shown in Fig. 3. Here, several positive CO_2 anomalies (SW quadrant of 3A and 3B) have formed ahead of the developing cyclone (NW quadrant of 3B) due, in this

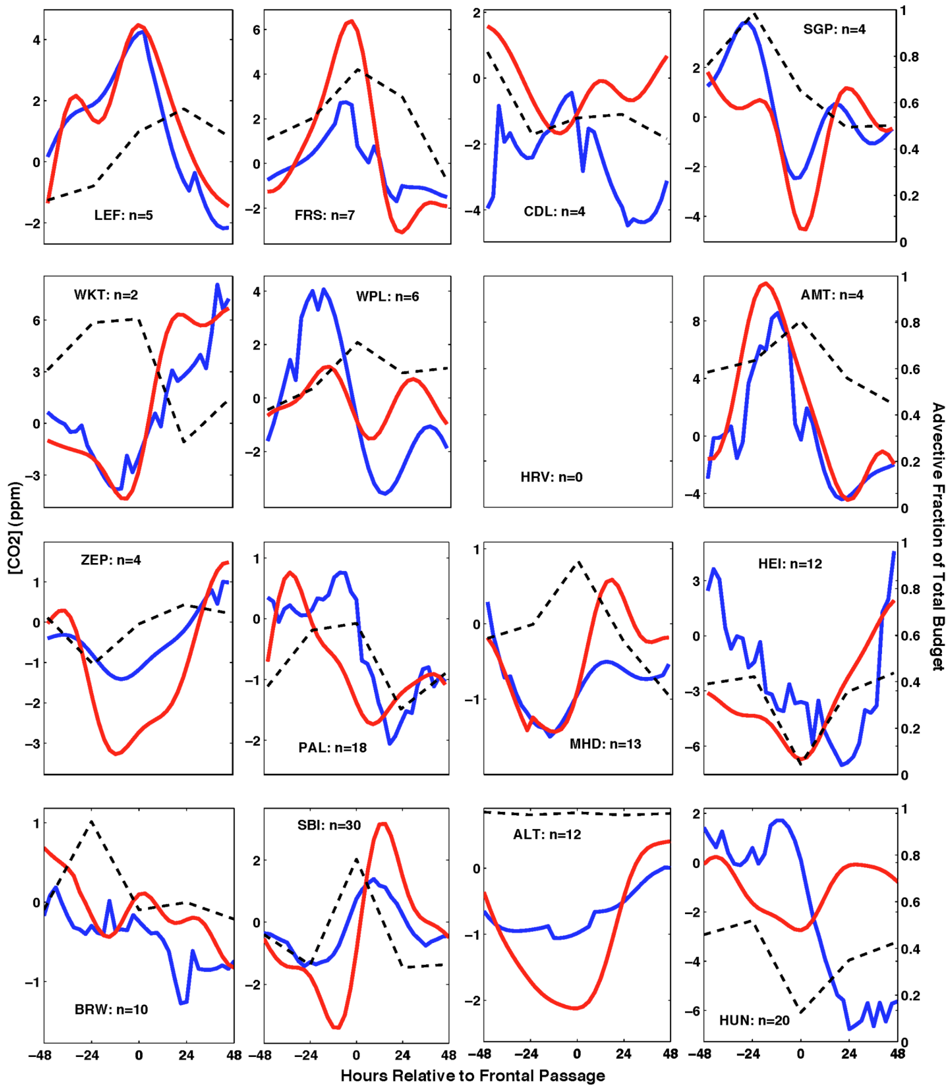

Fig. 5. Same as Fig. 4 except for Winter (November–December–January–Febraury).

case, to persistent positive NEE and advection of fossil fuel emissions from the east (not shown). The anomalies merge together in the wind shear south of the cyclone. On day 3 (3C) the anomalies align with the front and advect to the east during day 4 (3D). The preexisting NE-SW CO_2 gradient is organized and concentrated into a narrow frontal zone of high CO_2 by shearing and deformational flow.

In this example a traveling surface front creates important downstream variations. This example demonstrates the importance of fronts, through deformation flow and advection, for transporting remotely generated CO_2 anomalies, enhancing gradients, and causing variations that are non-local at sites thousands of kilometers away. Budget analysis in Sect. 3.3 shows the importance of advection during frontal passage. This same analysis is used in Sect. 3.4 to show that advection is largely responsible for many of the day-to-day variations seen in midlatitudes.

Cloudiness and precipitation are common along frontal transition zones. Evidence that CO_2 anomalies concentrate along this same zone presents a potential problem for satellite observations of column CO_2 because frontal anomalies are likely to be hidden under clouds (Corbin and Denning, 2006). Surface observations, which measure continuously in time, are a critical means for recording boundary layer variations along fronts, and therefore an important way to observe fluxes that occur for thousands of kilometers upstream. Continuous surface observations are therefore complementary to satellite observations, which observe much more continuously in space.

3.2 Frontal CO_2

This section provides model and observational evidence that fronts contribute to atmospheric variations regardless of local

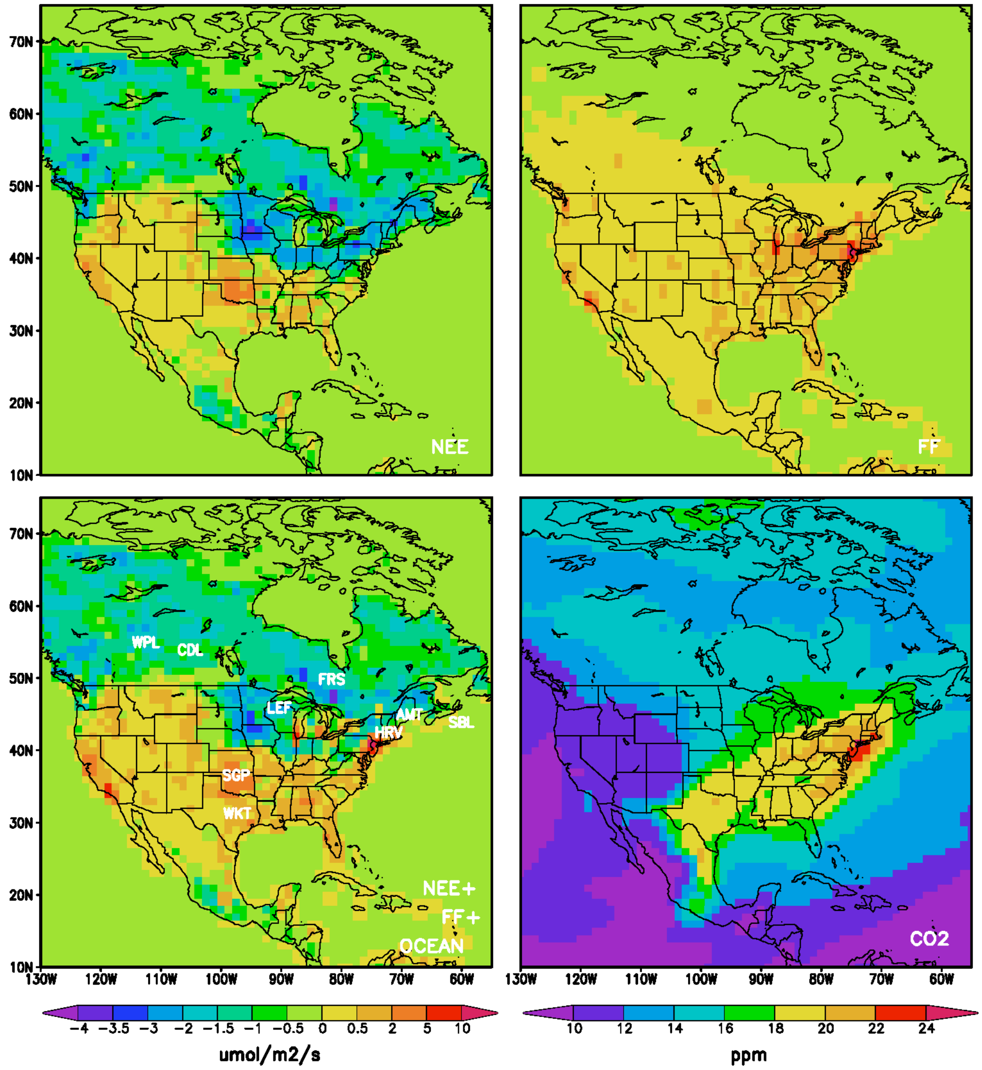

Fig. 6. July mean surface CO_2 flux of net ecosystem exchange (NEE, top left), fossil fuel emissions (FF, top right), total surface flux (NEE + FF + air-sea exchange (OCEAN), bottom left), and boundary layer CO_2 (bottom right) for North America. Plots of surface flux are on the same scale, with units of μmol/m^2/s, corresponding to the color bar on the bottom left. CO_2 is plotted in units of ppm, with the corresponding color bar on the bottom right. Locations of continuous sites are plotted in the bottom left plot for convenience.

surface flux. By averaging frontal CO_2 signals over multiple events, the importance of cold fronts for producing strong downstream variations is shown. These variations are shown to be persistent throughout the year. Additionally, comparison between simulated and observed CO_2 provides much information about strengths and weaknesses in the modeling system.

The procedure for creating frontal CO_2 climatologies is as follows. First, some general way of defining frontal zones in which frontal signals occur is needed. This study focuses on surface cold fronts in part because the surface signatures tend to be more sharply defined than in other fronts, making them easier to identify and study (Schultz, 2005). Surface fronts are characterized according to Renard and Clarke (1965), Holton (1992) and Hewson (1998), who consider fronts as warm-air boundaries of distinct thermal gradient separating two air-masses, defined by a first-order density discontinuity due to temperature and/or moisture contrasts and located on the warm-air side of the thermal gradient. This definition applies to density gradients in space and helps to locate surface fronts on weather maps. In this study, this definition is applied to density gradients in time, using temperature and water vapor as density proxies. These are used in conjunction with clockwise wind shifts and pressure minima to locate the warm-air boundary (Hewson, 1998; McCann and Whistler, 2001). Other frontal weather fields such as clouds, precipitation, and radiation are not used to classify fronts. Although important for NEE (e.g., Chan et al., 2004) such classification is beyond the scope of this study.

Table 2. Annual mean 3-hourly and day-to-day (mid-afternoon) budget tendencies (absolute values) due to horizontal advection (Horizontal), vertical advection (Vertical), moist convective transport (Cloud), and surface flux (Flux) for AMT, CDL, SGP, and TPJ. Each site includes 3-hourly (ppm/3 h) and daily (ppm/day) tendencies. The mean tendency is the first number of each box. Also included are annual standard deviations of the mean tendency (second value), and the percentage of the sum of tendencies (third value).

Station ID	Time	Horizontal	Vertical	Cloud	Flux
AMT	3-hourly	*0.39 (0.50) 14.5%*	*0.82 (1.07) 30.8%*	*0.06 (0.11) 2.1%*	*1.40 (1.17) 52.5%*
	daily	*1.76 (1.93) 20.0%*	*3.96 (3.90) 43.9%*	*0.33 (0.51) 3.7%*	*2.95 (2.47) 32.8%*
CDL	3-hourly	*0.15 (0.18) 16.8%*	*0.33 (0.39) 37.0%*	*0.02 (0.05) 2.7%*	*0.39 (0.45) 43.5%*
	daily	*0.65 (0.74) 19.6%*	*1.59 (1.62) 47.9%*	*0.17 (0.31) 5.2%*	*0.91 (0.84) 27.4%*
SGP	3-hourly	*0.32 (0.42) 13.1%*	*0.63 (0.73) 26.6%*	*0.09 (0.18) 3.6%*	*1.38 (1.08) 57.2%*
	daily	*1.53 (1.89) 18%*	*3.43 (3.19) 40.3%*	*0.52 (0.94) 6.1%*	*3.03 (2.02) 35.6%*
TPJ	3-hourly	*0.12 (0.15) 2.8%*	*0.34 (0.36) 7.6%*	*0.51 (0.51) 11.6%*	*3.47 (1.40) 78.1%*
	daily	*0.71 (0.76) 7.3%*	*1.85 (1.81) 19.0%*	*3.05 (3.27) 31.4%*	*4.08 (5.10) 42.1%*

Surface pressure and 10 m wind, temperature, and specific humidity from GEOS4-DAS are used at 3-hourly resolution to identify the time of frontal passage at the continuous CO_2 sites. Diurnal and seasonal cycles are removed from the temperature and specific humidity time series using a butterworth filter until only synoptic variations remain (1–5 days). The time of frontal passage is approximated using the "frontal locator function", described in McCann and Whistler (2001), as the time at which the function $GG\rho = {}^{\partial\rho}/_{\partial t} \cdot {}^{\partial}/_{\partial t} \left| {}^{\partial\rho}/_{\partial t} \right|$ minimizes over synoptic time scales, concurrent with a clockwise wind shift and approximate pressure minimum, where ρ is temperature or water vapor and || indicates the magnitude of the gradient of ρ. This function describes temporal gradients of the magnitude of temporal gradients of density (right side of dot product), with a negative dot product indicating the warm side edge of the frontal zone (see Fig. 3d of Renard and Clark, 1965 for application of a similar function in space).

After identifying particular events using the frontal locator function, frontal composites of CO_2 are constructed by averaging the filtered hourly data at each station from 48 h before frontal passage until 48 h after. The result is the average (observed and simulated) frontal signal that a station experiences as fronts pass by, with time increasing on the x-axis from left to right with zero representing the time of frontal passage and negative (positive) time anomalies representing the signal before (after) frontal passage (see Figs. 4 and 5).

Before discussing Figs. 4 and 5, it is important to note that Kawa et al. (2004), using PCTM driven by the $2^\circ \times 2.5^\circ$ version of GEOS4-DAS, show that the timing of transport events has a peak at zero lag in cross correlations of simulated and observed CO_2. A similar result is found in the work of Patra et al. (2008), who compare CO_2 simulations across a range of chemistry transport models, all driven by reanalyzed weather, and show that the strongest synoptic-scale correlations occur at zero time lag and in models using finer horizontal resolution. These findings provide evidence that the use of reanalyzed weather in offline chemistry transport models creates good agreement between simulated and observed transport events. The $1^\circ \times 1.25^\circ$ version of GEOS4-DAS used in this experiment is therefore expected to reproduce the timing and location of transport events in a realistic way.

Frontal CO_2 climatologies are shown in Figs. 4 and 5. These climatologies suggest that persistent variations are common, and that some sites (e.g., SGP, WKT, SBI, and WPL) feature air mass replacement of higher prefrontal CO_2 with lower postfrontal CO_2. At other sites CO_2 variations occur as transient spikes during frontal passage (e.g., CDL, AMT, and ZEP). Time-mean maps of surface flux and near-surface CO_2 combined with the constraint that all frontal events exhibit clockwise wind shifts characteristic of cold fronts (i.e., wind direction shift from southerly to northerly) helps to explain the nature of these signals and why they vary between sites. Figure 6 shows a very diverse pattern of terrestrial influence over North America unique to each site (site location plotted for convenience).

SGP and WKT, for example, exhibit a frontal signal in which CO_2 mixing ratios decrease over the course of frontal passage, concurrent with strong advection (see Fig. 4). According to Fig. 6, the region containing these sites is dominated by positive surface flux while the region to the north is dominated by negative surface flux. This creates a north-south gradient in surface flux which, when under the influence of fair weather typical of a high-pressure system, tends to create relatively CO_2 depleted air masses to the north and CO_2 enriched air masses to the south (see bottom right plot in Fig. 6). If a low-pressure system develops and air is advected from the north during frontal passage, as is expected from typical frontal wind patterns, the decreasing CO_2 tendency associated with frontal signals observed at SGP and WKT is explained. Unique upstream surface flux influence (each site is different), combined with deformational compression and strong advection along fronts (see Figs. 4, 5, and Sect. 3.3), explain the uniqueness and persistency of frontal climatologies.

Table 3. Same as Table 2 except for observed and total model tendencies.

Station ID	Time	Observed	Model
AMT	3-hourly	*4.75 (6.16)*	*2.60 (2.77)*
	daily	*2.88 (3.29)*	*3.62 (4.04)*
CDL	3-hourly	*3.15 (4.29)*	*0.88 (1.14)*
	daily	*1.90 (2.02)*	*1.66 (1.64)*
SGP	3-hourly	*6.06 (7.60)*	*2.85 (2.90)*
	daily	*3.75 (3.50)*	*3.08 (3.15)*
TPJ	3-hourly	*11.43 (9.14)*	*7.13 (4.22)*
	daily	*4.47 (4.55)*	*2.70 (4.02)*

Model-observation mismatches in Figs. 4 and 5 include differences in phase and amplitude. Some of these mismatches are attributed to surface boundary conditions. Although Patra et al. (2008) show that the use of constant in time and spatially coarse fossil fuel emissions in transport simulations produces realistic synoptic variations over continents, it is likely that time varying maps with finer spatial resolution produce more realistic simulations. It is common, for example, for fossil fuel emissions from cities to smear out over forests at the current resolution. This is a problem in the New England region and effectively results in CO_2 emissions from some forests, affecting both the phase and amplitude of frontal CO_2. Whether using a higher-resolution fossil fuel map improves correlations at synoptic scales, however, remains to be shown.

A more extreme example of sensitivity to boundary conditions is HEI. Large errors occur at HEI because contamination by local fossil fuel emissions is strong. Such strong point sources are not included in the simulations. Sensitivity to local contamination is magnified in the winter when concentrations near the surface are less likely to mix vertically. This effect is seen in Fig. 1, with day-to-day variability strongest during winter months.

Another possible explanation for amplitude errors is the representation of ecosystem respiration, which is scaled to balance gross primary production, and the assumption of annually balanced surface flux. In regions where long-term sinks exist in nature, SiB3 estimates of surface flux are too positive and CO_2 concentrations are overestimated.

Patra et al. (2008) show sensitivity of synoptic correlations of modeled CO_2 to a variety of other factors, including: (1) the use of 6-hourly wind fields, as used in this study, compared to 3-hourly; (2) season, such that CO_2 correlations were generally strongest (weakest) during the winter (summer); (3) site location, with the greatest correlations at lower altitude continental sites surrounded by homogeneous terrain; and (4) the choice of land surface model as terrestrial biosphere flux. The time resolution of meteorology affects the timing of frontal passage and therefore the phase of frontal CO_2 signals. Sensitivity to season and site location is evident in the CO_2 climatologies. Sensitivity to land surface model affects synoptic correlations year round and is strongest at continental sites.

3.3 Budget analysis

Overall, PCTM reproduces much of the amplitude, shape, and phase of the observed composite surface signals in Figs. 4 and 5. The discussion therefore turns to analysis of model output to understand the role of physical and biological mechanisms along fronts in creating the frontal CO_2 signatures discussed above. Previous studies discuss the existence of advection, NEE, and moist convection along fronts; there have been few attempts, however, to quantify the role of each mechanism in a systematic way to explain the strong and sudden variations shown, for example, in Figs. 1, 4, and 5. Diagnosis of simulated tendencies associated with frontal climatologies illustrates the importance of advection compared to surface flux and moist convection during frontal passage. Equation (1)

$$\underbrace{\frac{\partial C}{\partial t}}_{i} + \underbrace{\frac{RT}{p}\frac{F_c}{z_1}}_{ii} + \underbrace{K_m\frac{\partial C}{\partial z}}_{iii} + \underbrace{W\frac{\partial C}{\partial z}}_{iv} + \underbrace{\vec{\boldsymbol{V}}_{\boldsymbol{H}} \times \nabla_H C}_{v} + \underbrace{g\frac{M\partial C}{\partial p}}_{vi} = 0 \tag{1}$$

represents the simulated CO_2 tendency (i) due to surface flux (ii), vertical diffusion (iii), vertical advection (iv), horizontal advection (v), and vertical cloud transport (vi), where C is CO_2 mixing ratio in ppm, F_c is the surface flux due to NEE, fossil fuel emissions, and air-sea exchange, z_1 is the lowest model level (~50 m), R is the gas constant, T is temperature, p is pressure, K_m is the vertical diffusion coefficient, W is vertical velocity, $\vec{\boldsymbol{V}}_{\boldsymbol{H}}$ is the horizontal wind, g is gravity, and M is net convective mass flux as described in the work of Kawa et al. (2004).

To gauge relative importance, the tendencies are output from PCTM every hour. Terms (ii) and (iii) together represent vertical diffusion of surface flux. This process is represented by two steps within PCTM: In step 1, surface flux acts over the lowest model layer (z_1) through term (ii); in step 2, CO_2 is mixed vertically by the vertical diffusion coefficient through term (iii) such that surface fluxes are exposed vertically through the atmosphere. Hourly tendencies at each layer within the PBL are averaged through the three lowest model levels (approximately representing the lowest 500m of the PBL) and then converted to daily and three-hourly tendencies. Daily tendencies are calculated from 12:00 p.m. of day 1 to 12:00 p.m. of the next day (local time) to represent day-to-day (synoptic) influence on PBL concentrations. To represent the relative influence of each term, individual tendencies (terms of Eq. 1) are divided by the total tendency (sum of terms in Eq. 1). Annual mean percent contributions at several sites in North and South America are shown in Table 2. These values are discussed in more detail in Sect. 3.4.

Here, budget tendencies associated with frontal passage are discussed. The dashed lines in Figs. 4 and 5 show the relative influence of horizontal plus vertical advection on frontal CO_2 tendencies. In these plots, the fractional contribution of advection is averaged across the same events used in the frontal climatologies. This budget analysis suggests that the 24-hour advective tendency is approximately 60% during frontal passage in the summer, ranging from about 30% where total local surface flux (NEE + fossil fuel emissions) tendencies are strongest (e.g., FRS and PAL) to above 75% where advection dominates (coastal sites such as MHD, ZEP and SBI and remote regions such as BRW and ALT). Vertical cloud transport accounts for about 8% of frontal CO_2 tendencies on average. Advection accounts for a larger percentage in the winter (69%) when NEE is weak.

In the analysis above, 60% of midlatitude frontal variations are attributed to horizontal and vertical transport through air mass exchange and deformational flow. This is not so in Amazonia, where baroclinic disturbance is less prevalent, yet CO_2 variations during the rainy season are as large as midlatitude variations, suggesting the presence of other sources for variability. Mechanisms for variations at a site in Amazonia are analyzed below.

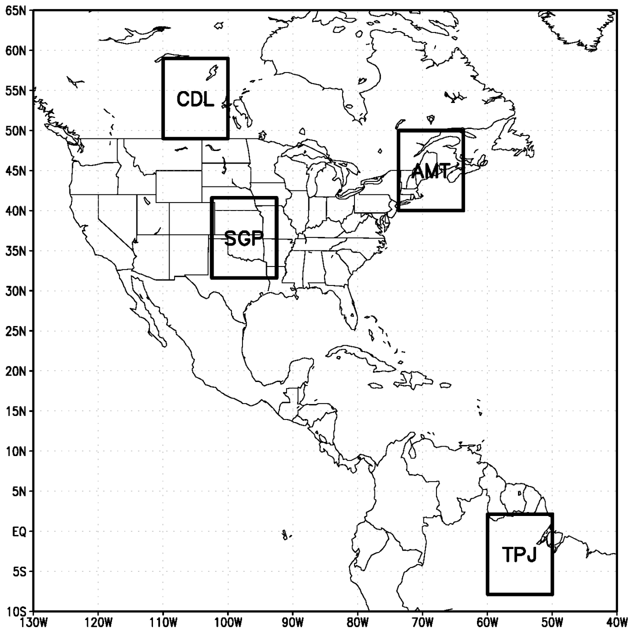

Fig. 7. Domains used for NOFLUX, NOCONV, and RADCLIM sensitivity experiments. Grid cells at the center of each domain are used for analysis. The same grid cells are used in analysis of the VERTMIX experiment.

3.4 Midlatitude vs tropical mechanisms

Sensitivity of tropical and midlatitude CO_2 to local/regional and global processes is assessed with simple modeling experiments designed to test changes in day-do-day variability in response to meteorological and flux parameters varied about their control values. For the control run, denoted CONTROL, PCTM is employed as described in Sect. 2. Three sensitivity experiments are performed in which transport and surface flux fields are modified within 10° square domains centered at grid cells in Amazonia (TPJ: 3° S, 55° W) and in midlatitudes (CDL: 54° N, 105° W, SGP: 37° N, 97.5° W, and AMT: 45° N, 69° W). The domains are shown in Fig. 7.

In the first experiment, NOCONV, sensitivity to moist convective transport is assessed by running PCTM for one year with cloud mass flux (CMF) set to zero in the 10° domains. Cloud-radiative NEE forcing still occurs offline in SiB3, but atmospheric mixing by CMF in PCTM does not. In a second experiment, NOFLUX, sensitivity to surface flux is tested by setting fluxes of NEE and fossil fuel emissions to zero in the same 10° domains. Transport parameters are held at control values in this experiment. In the third experiment, RADCLIM, surface flux variations associated with photosynthetically active radiation and cloud cover are tested by driving offline SiB3 with climatological solar radiation. This climatology is calculated using a 30-day running mean of 3-hourly shortwave radiation from GEOS4-DAS. Again, transport is unmodified.

An additional experiment, VERTMIX, varies the vertical diffusion coefficient and CMF about their control values over the entire globe (all time, all vertical levels, and all grid points), while keeping surface flux at control values, to assess larger scale impacts of vertical mixing on local CO_2 variations. VERTMIX consists of four runs: (1) CMF is doubled (denoted *twice_cmf*), (2) CMF is halved (denoted *half_cmf*), (3) vertical diffusion coefficient is doubled (denoted *twice_vdif*), and (4) vertical diffusion coefficient is halved (denoted *half_vdif*). This experiment is used to evaluate vertical mixing and results from NOCONV.

Some terminology must be defined and justified. The four budget terms of interest for this analysis are horizontal advection, vertical advection, cloud transport, and surface flux, as described in Sect. 3.3. Non-local dynamics are defined as regional synoptic processes acting on the 10° domains that help to cause variations at the designated sites within these domains. These terms include horizontal and vertical advection, which are controlled by synoptic meteorology and transport CO_2 anomalies laterally and vertically. Local dynamics are defined as mesoscale processes that act within the 10° domains and cause variations local to a grid cell. These include moist convection and surface flux.

RADCLIM experiences little to no change in day-to-day variability compared to CONTROL, suggesting insensitivity to variations in shortwave radiation associated with clouds. This is not to say that NEE is unaffected by daily fluctuations in radiation, only that the simulated changes aren't

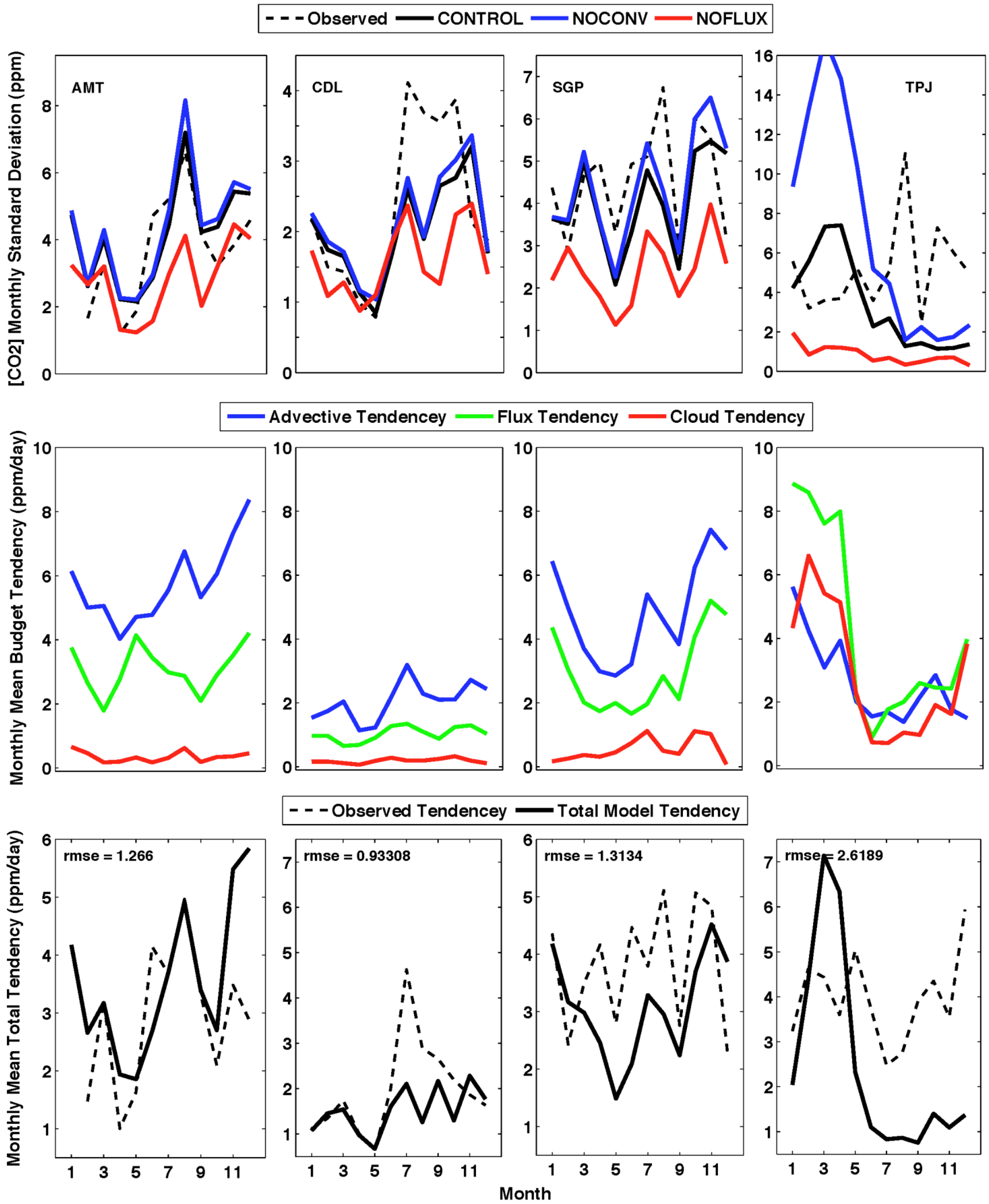

Fig. 8. Results from sensitivity experiments. (Top row) Monthly standard deviation of mid-afternoon CO_2 at grid cells containing AMT (far left column), CDL (second), SGP (third) and TPJ (far right) for observations (black), CONTROL (green), NOCONV (blue), and NOFLUX (red). (Second row) Monthly mean budget tendencies for advection (horizontal plus vertical advection, blue), surface flux (green), and moist convective transport (red) using CONTROL. (Third row) Monthly mean total tendency for observations (dashed) and CONTROL (solid). The root-mean-squared-error of the monthly standard deviations is shown for each station. All plots are on same monthly x-scale of the bottom row for one year, using monthly averaged values.

large enough to create a noticeable impact on variations in CO_2. Figure 8 (top row) shows monthly standard deviations of mid-afternoon observed and simulated CO_2 for each site and run, excluding RADCLIM since it is nearly identical to CONTROL and doesn't show up in the plot. Contrary to RADCLIM, NOFLUX causes standard deviations to decrease by as much as half relative to CONTROL at each site, and by more than half at TPJ such that local variations are greatly reduced. In NOCONV, variations are insensitive to moist convection at the midlatitude sites (except in the winter at SGP) and strongly sensitive at TPJ. These simulations show that variations at a site in Amazonia are more sensitive to local surface flux and moist convection than variations at midlatitudes sites. Despite excluding local surface flux in one experiment and moist convection in the other, strong midlatitude variations are retained in both cases, implying that advection is creating variations in the absence of local processes.

The second row of Fig. 8 shows monthly mean budget tendencies of advection (vertical + horizontal), surface flux and cloud transport for CONTROL. These plots demonstrate that CO_2 advection contributes more to variability in midlatitudes than does moist convective transport and that moist convection contributes more than horizontal advection at the Amazonian site. Table 2 quantifies annual mean tendencies for each term of the budget equation at each site. These values are calculated from the absolute values of 3-hourly and day-to-day tendencies.

A notable difference exists between 3-hourly and day-to-day tendencies, with transport tendencies decreasing and surface flux tendencies increasing from the 3-hourly to the day-to-day metric. This is attributed to the strong influence of surface flux on the diurnal cycle. The distribution due to synoptic processes is rather revealing in the day-to-day tendencies; the numbers illustrate a discrepancy between the midlatitudes and Amazonia in advection, moist convective transport, and surface flux. These numbers, based on the budget equation, show that advective CO_2 tendencies are much weaker (horizontal + vertical = 63% on average in midlatitudes and 26.3% at TPJ), the influence of moist convective transport much stronger (5% in midlatitudes and 31.4% at TPJ), and CO_2 tendencies due to surface flux slightly stronger (31.9% in midlatitudes and 42.1% at TPJ) at the Amazonian site. The standard deviation is, to first order, approximately proportional to the magnitude of the average tendency, indicating much variety in the dominant terms, and weaker variety in the weaker terms.

The bottom row of Fig. 8 shows a measure of uncertainty of the total model tendency, given by plots of monthly mean observed and total model day-to-day tendency for each station, together with the root-mean-squared-error. Additionally, Table 3 shows annual mean observed and total model tendency. These plots combined with values from Table 3 show that the control simulation is more accurate at the midlatitude sites than in Amazonia, in strength and seasonality. Simulated variations at TPJ are too strong from February–April (wet season) and too weak from August–December (late dry season – beginning of wet season). Comparison of observed and simulated NEE with vertically integrated CMF at TPJ helps to explain these mismatches (not shown), where overestimated NEE (too large and positive) during the end of the wet season combined with suppressed CMF causes enhanced CO_2 variations, as suggested in NOCONV experiments. Furthermore, SiB3 simulates a transition from net negative to net positive NEE from October–December while observations show persistent strong uptake. Such periods of neutral NEE, as suggested in NOFLUX simulations, promotes strongly suppressed CO_2 variations.

There are known errors in SiB3 estimates of NEE in Amazonia. These errors have been addressed in point simulations at TPJ in Baker et al. (2008). To create a more realistic situation of enhanced uptake during the wet season, deeper soils and a parameterization for hydraulic redistribution were added. The seasonality of simulated precipitation matches well with observations, indicating that the seasonality of moist convective mixing is realistic and that much of the error is likely due to surface flux. Additional tropical observations, improved land surface simulations, and improved representation of moist convection are ways to reduce uncertainty in the Amazonia in future experiments.

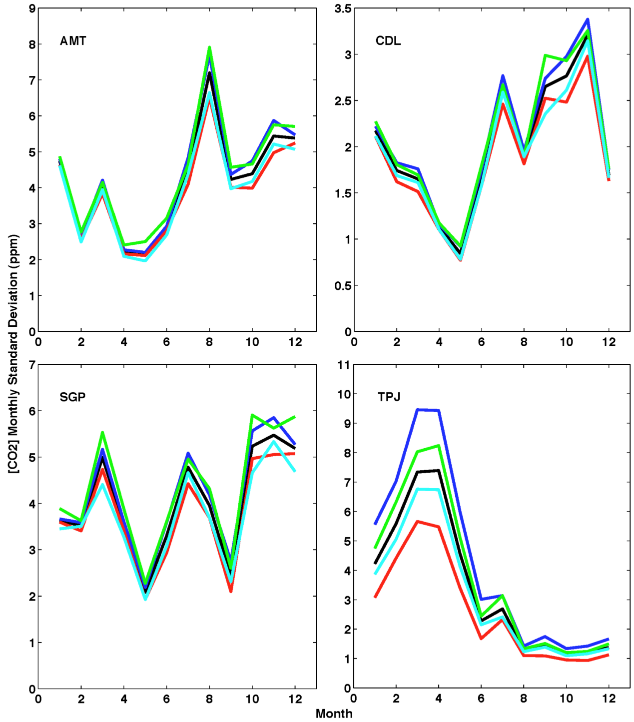

Fig. 9. Comparison of monthly standard deviation of mid-afternoon CO_2 from VERTMIX experiments (color) to CONTROL simulation (black) at grid cells containing AMT (top left), CDL (top right), SGP (bottom left), and TPJ (bottom right). VERTMIX experiments include *half_cmf* (blue), *twice_cmf* (red), *half_vdif* (green), and *twice_vdif* (cyan).

Figure 9 shows monthly standard deviations of mid-afternoon CO_2 from CONTROL and VERTMIX at CDL, AMT, SGP, and TPJ, similar to the top row of Fig. 8. Figure 8 shows insensitivity of day-to-day variations in midlatitudes to local/regional CMF in midlatitudes. Figure 9 shows that increasing or decreasing vertical mixing parameters such as CMF and VDIF over the entire globe does little to midlatitude variations. Seasonal patterns are similar to CONTROL; this is not surprising since vertical mixing in midlatitudes acts to smooth pre-established gradients rather than create new minima or maxima. The greatest changes in magnitude occur in the summer at SGP and the winter at AMT. Variations at TPJ, on the other hand, show much stronger sensitivity to vertical mixing compared to midlatitude sites, with enhanced (suppressed) variability in the presence of suppressed (enhanced) mixing, proportional to the magnitude of CO_2

variability in CONTROL (most pronounced during wet season). The spread of variability between the four runs is much greater at TPJ and suggests stronger sensitivity. These results are consistent with those of NOCONV. In all cases, variations are enhanced (suppressed) when vertical mixing is suppressed (enhanced).

These experiments confirm different simulated physical controls on day-to-day CO_2 variations in the midlatitudes and Amazonia. Important controls in midlatitudes are local (surface flux = 32% on average at the three North American sites) and non-local (horizontal and vertical advection combined account for 63% on average), with moist convective transport contributing only 5% on average. Variations at a site in Amazonia, on the other hand, are more strongly sensitive to local processes in our simulations in which clouds (31% of total) and surface flux (42%) dominate over advection (27%) in the annual budget. These budget contributions strongly imply coupling of local processes where PBL CO_2 recharges from surface fluxes and discharges vertically through convective transport. In these simulations, this is particularly true during the wet season (∼December–April), where simulated NEE is typically positive (Baker et al., 2008). Simulated CO_2 variability more than doubles in NOCONV and is strongly damped in NOFLUX. Advective transport in Amazonia must be occurring frequently enough, however, to prevent boundless CO_2 growth in NOCONV.

4 Summary and conclusions

According to continuous in-situ observations in North America, South America, and Europe, strong synoptic variations occur year round. Transport simulations suggest that atmospheric circulation differences cause different physical controls on variations in midlatitude and tropical regions. Analysis of observed and simulated summer frontal CO_2 climatologies shows that cold fronts contain information about upstream surface fluxes and regional scale gradients of CO_2 and are therefore an important source of CO_2 variability. Comparison of frontal CO_2 provides information about potential model improvements that can be made to achieve better representation of transport events.

In a frontal case study, deformational flow along fronts creates and maintains strong CO_2 contrasts, creating anomalous signals that advect along fronts. These frontal anomalies are likely to be hidden under clouds due to moist convection associated with fronts. Well-calibrated, in-situ continuous continental CO_2 measurements are, therefore, a required complement to satellite observations in midlatitudes because they contain the only observable signal from thousands of kilometers of upstream biogeochemistry.

Physical and biological mechanisms in the midlatitudes and Amazonia responsible for strong observed synoptic CO_2 variations are compared and quantified. Boundary layer budget analysis, combined with cloud and surface flux sensitivity experiments, provides evidence that regional scale advection is a major source for synoptic CO_2 variability in midlatitudes, whereas strong coupling between convective transport and surface flux is most important in Amazonia, where baroclinically induced synoptic transport is much weaker. With more continuous CO_2 observations available in the tropics, future work should extend the mechanistic analysis to additional Amazonian and tropical locations to help determine whether these conclusions can be generalized or not.

With regard to assessments of the global and tropical carbon budget, budget analysis and sensitivity simulations demonstrate the need for carbon cycle models to properly represent moist convection, surface flux, and their dynamical interactions in Amazonia. The importance of moist convective transport implies that CO_2 anomalies created within the boundary layer are transported to the upper troposphere by moist convection and hidden from surface towers, and, with regard to inverse modeling, need to be accounted for either with proper modeling techniques and/or through upper air CO_2 observations. These in-situ observations are critical in the tropics where clouds and moist convection hide surface variations from satellite observations.

The dominance of advection in midlatitudes implies that the use of reanalyzed winds for global transport simulations is critical for reliable simulations and accurate inverse surface flux estimates. Surface flux, however, contributes nearly 30% on average to day-to-day variations at the surface, and it is therefore important for transport models to use sub-daily resolution estimates of land surface flux to reproduce the full extent of high-frequency CO_2 variations. Although some sensitivity to radiation is demonstrated during the growing season at midlatitude sites, sensitivity is weak on annual average. Surface flux, in general, is more important during fair weather days when advection is weaker.

Acknowledgements. This research would not been possible without data providers. We thank Margaret Torn, Sebastien Biraud, and Marc Fischer at LBNL for SGP, William Munger and Steve Wofsy at Harvard University for HRV and TPJ, Arlyn Andrews at NOAA/ESRL/GMD for LEF, WKT, and AMT, Douglas Worthy at MSC for CDL, FRS, ALT, and SBI, Larry Flanagan at the University of Lethbridge for WPL, Philippe Ciais and Leonard Rivier for their work in the Carboeurope Database, Johan Strom at SU for ZEP, Tuula Aalto at FMI for PAL, Ingeborg Levin at UHEI-IUP for HEI, Michel Ramonet at CEA-LSCE for MHD, Laszlo Haszpra and Zoltan Barcza for HUN, and WMO WDCGG and NOAA/ESRL/GMD for making CO_2 data publicly available. We also thank the editor and anonymous reviewers for constructive comments and recommendations. This research is supported by the National Aeronautics and Space Administration Contracts #NNX06AC75G, #NNG05GD15G, #NNG05GF41G, #NNX08AM56G, and #NNG06GB41G.

Edited by: H. Wernli

References

Andres, R. J., Marland, G., Fung, I., and Matthews, E.: A 1 degrees $\times$ 1 degrees distribution of carbon dioxide emissions from fossil fuel consumption and cement manufacture, 1950–1990, Global Biogeochem. Cy., 10, 419–429, 1996.

Baker, I. T., Denning, A. S., Hanan, N., Prihodko, L., Vidale, P.-L., Davis, K., and Bakwin, P.: Simulated and observed fluxes of sensible and latent heat and CO_2 at the WLEF-TV Tower using SiB2.5, Global Change Biol., 9, 1262–1277, 2003.

Baker, D. F., Law, R. M., Gurney, K. R., Rayner, P., et al.: TransCom 3 inversion intercomparison: Impact of transport model errors on the interannual variability of regional CO_2 fluxes, 1988–2003, Global Biogeochem. Cy., 20, GB1002, doi:10.1029/2004GB002439, 2006.

Baker, I. T., Prihodko, L., Denning, S., Goulden, M., Miller, S., and Da Rocha, H. R.: Seasonal drought stress in the Amazon: Reconciling models and observations, J. Geophys. Res., 113, G00B01, doi:10.1029/2007JG000644, 2008.

Bakwin, P. S., Tans, P. P., Hurst, D. F., and Zhao, C.: Measurements of carbon dioxide on very tall towers: results of the NOAA/CMDL program, Tellus, 50B, 401–415, 1998.

Barford, C. C., Wofsy, S. C., Goulden, M. L., Munger, J. W., Pyle, E. H., et al.: Factors controlling long- and short-term sequestration of atmospheric CO_2 in a mid-latitude forest, Science, 294, 2415–2434, 2001.

Biraud, S., Ciais, P., Ramonet, M., Simmonds, P., Kazan, V., Monfray, P., O'Doherty, S., Spain, G., and Jennings, S. G.: Quantification of carbon dioxide, methane, nitrous oxide and chloroform emissions over Ireland from atmospheric observations at Mace Head, Tellus, 54B, 41–60, 2002.

Bloom, S., da Silva, A., and Dee, D.: Documentation and validation of the Goddard Earth Observing System (GEOS) Data Assimilation System, Version 4, Technical Report Series on Global Modeling and Data Assimilation, Greenbelt, MD, 2005.

Chan, D., Yuen, C. W., Higuchi, K., Shashkov, A., Liu, J., Chen, J., and Worthy, D.: On the CO_2 exchange between the atmosphere and the biosphere: the role of synoptic and mesoscale processes, Tellus, 56B, 194–212, 2004.

Corbin, K. D. and Denning, A. S.: Using continuous data to estimate clear-sky errors in inversion of satellite CO_2 measurements, Geophys. Res. Lett., 33, LI2810, doi:10.1029/2006GL025910, 2006.

Dai, Y., Zeng, X., Dickinson, R. E., Baker, I., et al.: The common land model, Bull. Amer. Meteorol. Soc., 84, 1013–1023, 2003.

Davis, K. J., Bakwin, P. S., Yi, C., Berger, B. W., Zhao, C., Teclaw, R. M., and Isebrands, J. G.: The annual cycle of CO_2 and H_2O exchange over a northern mixed forest as observed from a very tall tower, Global Change Biol., 9, 1278–1293, 2003.

Denning, A. S., Collatz, J. G., Zhang, C., Randall, D. A., Berry, J. A., Sellers, P. J., Colello, G. D., and Dazlich, D. A.: Simulations of terrestrial carbon metabolism and atmospheric CO_2 in a general circulation model – Part 1: Surface carbon fluxes, Tellus, 48B, 521–542, 1996.

Eneroth, K., Aalto, T., Hatakka, J., Holmen, K., Laurila, T., and Viisanen, Y.: Atmospheric transport of carbon dioxide to a baseline monitoring station in northern Finland, Tellus, 57B, 366–374, 2005.

Gamnitzer, U., Karstens, U., Kromer, B., Neubert, R. E. M., Meijer, H. A. J., Schroeder, H., and Levin, I.: Carbon monoxide: A quantitative tracer for fossil fuel CO_2, J. Geophys. Res., 111, D22302, doi:10.1029/2005JD006966, 2006.

Geels, C., Doney, S. C., Dargaville, R., Brandt, J., and Christensen, J. H.: Investigating the sources of synoptic variability in atmospheric CO_2 measurements over the Northern Hemisphere continents: a regional model study, Tellus, 56B, 35–50, 2004.

Gerbig, C., Lin, J. C., Wofsy, S. C., Daube, B. C., Andrews, A. E., Stephens, B. B., Bakwin, P. S., and Grainger, C. A.: Toward constraining regional-scale fluxes of CO_2 with atmospheric observations over a continent: 2. Analysis of COBRA data using a receptor-oriented framework, J. Geophys. Res., 108(D24), 4757, doi:10.1029/2003JD003770, 2003.

Goulden, M. L., Miller, S. D., da Rocha, H. R., Menton, M. C., de Freitas, H. C., e Silva Figueira, A. M., and de Sousa, C. A. D.: Diel and seasonal patterns of tropical forest CO_2 exchange, Ecol. Appl., 14(4), supplement, S42–S54, 2004.

Gurney, K. R., Law, R. M., Denning, A. S., Rayner, P. J., et al.: Towards robust regional estimates of CO_2 sources and sinks using atmospheric transport models, Nature, 415, 626–630, 2002.

Gurney, K. R., Law, R. M., Denning, A. S., Rayner, P. J., et al.: TransCom 3 CO_2 inversion intercomparison: 1. Annual mean control results and sensitivity to transport and prior flux informatin, Tellus, 55B, 555–579, 2003.

Hack, J. J.: Parameterization of moist convection in the National Center for Atmospheric Research community climate model (CCM2), J. Geophys. Res., 99, 5551–5568, 1994.

Hanan, N. P., Berry, J. A., Verma, S. B., Walter-Shea, E. A., Suyker, A. E., Burba, G. G., and Denning, A. S.: Testing a model of CO_2, water and energy exchange in Great Plains tall-grass prairie and wheat ecosystems, Agr. Forest Meteorol., 131, 162–179, 2005.

Haszpra, L., Barcza, Z., Bakwin, P. S., Berger, B. W., Davis, K. J., and Weidinger, T.: Measuring system for the long-term monitoring of biosphere/atmosphere exchange of carbon dioxide, J. Geophys. Res., 106D, 3057–3070, 2001.

Hewson, T. D.: Objective fronts, Meteorol. Appl., 5, 37–65, 1998.

Higuchi, K., Worthy, D., Chan, D., and Shashkov, A.: Regional source/sink impact on the diurnal, seasonal and inter-annual variations in atmospheric CO_2 at a boreal forest site in Canada, Tellus, 55B, 115–125, 2003.

Holton, J. R.: An Introduction to Dynamic Meteorology, Third Edition, Elsevier, San Diego, CA, USA, 368–369, 267 pp., 1992.

Huffman, G. J., Adler, R. F., Morrissey, M., Bolvin, D. T., Curtis, S., Joyce, R., McGavock, B., and Susskind, J.: Global precipitation at one degree daily resolution from multi-satellite observations, J. Hydrometeor., 2, 36–50, 2001.

Kawa, S. R., Erickson III, D. J., Pawson, S., and Zhu, Z.: Global CO_2 transport simulations using meteorological data from the NASA data assimilation system, J. Geophys. Res., 109, D18312, doi:10.1029/2004JD004554, 2004.

Kiehl, J. T., Hack, J. J., Bonan, G. B., Boville, B. A., Williamson, D. L., and Rasch, P. J.: The National Center for Atmospheric Research Community Climate Model: CCM3, J. Climate, 11, 1131–1149, 1998.

Lauvaux, T., Uliasz, M., Sarrat, C., Chevallier, F., Bousquet, P., Lac, C., Davis, K. J., Ciais, P., Denning, A. S., and Rayner, P. J.: Mesoscale inversion: first results from the CERES campaign with synthetic data, Atmos. Chem. Phys., 8, 3459–3471, 2008, http://www.atmos-chem-phys.net/8/3459/2008/.

Law, R. M., Rayner, P. J., Steele, L. P., and Enting, I. G.: Using high temporal frequency data for CO_2 inversions, Global Biogeochem. Cy., 16(4), 1053, doi:10.1029/2001GB001593, 2002.

Law, R. M., Peters, W., Rödenbeck, C., Aulagnier, C., et al.: TransCom model simulations of hourly atmospheric CO_2: Experimental overview and diurnal cycle results for 2002, Global Biogeochem. Cy., 22, GB3009, doi:10.1029/2007GB003050, 2008.

Lin, J. C., Gerbig, C., Wofsy, S. C., Andrews, A. E., Daube, B. C., Grainger, C. A., Stephens, B. B., Bakwin, P. S., and Hollinger, D. Y.: Measuring fluxes of trace gases at regional scales by Lagrangian observations: Application to the CO_2 Budget and Rectification Airborne (COBRA) study, J. Geophys. Res., 109, D15304, doi:10.1029/2004JD004754, 2004.

Lin, S. J. and Rood, R. B.: Multidimensional flux-form semi-Lagrangian transport schemes, Mon. Weather Rev., 124, 2046–2070, 1996.

McCann, D. W. and Whistler, J. P.: Problems and solutions for drawing fronts objectively, Meteorol. Appl., 8, 195–203, 2001.

NOAA GMD Carbon Cycle Greenhouse Gases Group, online available at: http://www.esrl.noaa.gov/gmd/ccgg/index.html, March 2008.

Patra, P. K., Law, R. M., Peters, W., Rödenbeck, C., et al.: TransCom model simulations of hourly atmospheric CO_2: analysis of synoptic scale variations for the period 2002–2003, Global Biogeochem. Cy., 22, GB4013, doi:10.1029/2007GB003081, 2008.

Peylin, P., Rayner, P. J., Bousquet, P., Carouge, C., Hourdin, F., Ciais, P., Heinrich, P., and AeroCarb Contributors: Daily CO_2 flux estimate over Europe from continuous atmospheric measurements: Part 1 inverse methodology, Atmos. Chem. Phys., 5, 3173–3186, 2005, http://www.atmos-chem-phys.net/5/3173/2005/.

Renard, R. J. and Clarke, L. C: Experiments in numerical objective frontal analysis, Mon. Weather Rev., 93, 547–556, 1965.

Rödenbeck, C., Houweling, S., Gloor, M., and Heimann, M.: CO_2 flux history 1982–2001 inferred from atmospheric data using a global inversion of atmospheric transport, Atmos. Chem. Phys., 3, 1919–1964, 2003, http://www.atmos-chem-phys.net/3/1919/2003/.

Schultz, D. M.: A review of cold fronts with prefrontal troughs and wind shifts, Mon. Weather Rev., 133, 8, 2449–2472, 2005.

Sellers, P. J., Mintz, Y., Sud, Y. C., and Dalcher, A.: A simple biosphere model (SiB) for use within general circulation models, J. Atmos. Sci., 43, 505–531, 1986.

Sellers, P. J., Randall, D. A., Collatz, G. J., Berry, J. A., Field, C. B., Dazlich, D. A., Zhang, C., Collelo, G. D., and Bounoua, L.: A revised land-surface parameterization (SiB2) for atmospheric GCMs – Part 1: Model formulation, J. Climate, 1, 676–705, 1996.

Sims, P. L. and Bradford, J. A.: Carbon dioxide fluxes in a southern plains prairie, Agr. Forest Meteorol., 109, 117–134, 2001.

Stohl, A., Berg, T., Burkhart, J. F., Fjraa, A. M., et al.: Arctic smoke – record high air pollution levels in the European Arctic due to agricultural fires in Eastern Europe in spring 2006, Atmos. Chem Phys., 7, 511–534, 2007.

Syed, K. H., Flanagan, L. B., Carlson, P. J., Glenn, A. J., and Van Gaalen, K. E.: Environmental control of net ecosystem CO_2 exchange in a treed, moderately rich fen in northern Alberta, Agr. Forest Meteorol., 140, 97–114, 2006.

Takahashi, T. S., Sutherland, S. C., Sweeney, C., Poisson, A., et al.: Global Sea-Air CO_2 flux based on climatological surface ocean pCO_2 and seasonal biological and temperature effects, Deep-Sea Research Part II, 49, 1601–1622, 2002.

Vidale, P. L. and Stockli R.: Prognostic canopy air space solutions for land surface exchanges, Theor. Appl. Climatol., 80, 245–257, 2005.

Wang, J.-W., Denning, A. S., Lu, L., Baker, I. T., Corbin, K. D., and Davis, K. J.: Observations and simulations of synoptic, regional, and local variations in atmospheric CO_2, J. Geophys. Res., 112, D04108, doi:10.1029/2006JD007410, 2007.

World Data Centre for Greenhouse Gases (WDCGG): http://gaw.kishou.go.jp/wdcgg/, June 2008.

Worthy, D. E., Levin, I., Trivett, N. B., Kuhlmann, A. J., Hopper, J. F., and Ernst, M. K.: Seven years of continuous methane observations at a remote boreal site in Ontario, Canada, J. Geophys. Res., 103, D13, 15 995–16 007, 1998.

Worthy, D. E., Higuchi, K., and Chan, D.: North American influence on atmospheric carbon dioxide data collected at Sable Island, Canada, Tellus, 55B, 105–114, 2003.

Zhang, G. J. and McFarlane, N. A.: Sensitivity of climate simulations to the parameterizations of cumulus convection in the Canadian climate center general-circulation model, Atmos. Ocean, 33, 407–446, 1995.